EPJ Photovoltaics **11**, 8 (2020)

https://doi.org/10.1051/epjpv/2020005

Available online at:
www.epj-pv.org

REGULAR ARTICLE OPEN ACCESS

Impact of RbF-PDT on Cu(In,Ga)Se_2 solar cells with CdS and Zn(O,S) buffer layers

Ana Kanevce*, Stefan Paetel, Dimitrios Hariskos, and Theresa Magorian Friedlmeier

Zentrum für Sonnenenergie- und Wasserstoff- Forschung, Meitnerstraße 1, 70563 Stuttgart, Germany

Received: 15 July 2020 / Received in final form: 15 September 2020 / Accepted: 17 September 2020

Abstract. Alkali-fluoride post-deposition treatments (PDTs) of Cu(In,Ga)Se_2 (CIGS) absorbers have repeatedly resulted in device efficiency improvements, observed mainly due to an open-circuit voltage (V_{oc}) enhancement. Replacement of the CdS buffer layer with a higher band gap alternative can increase the short-circuit current density (J_{sc}) and also eliminate the use of Cd. In many alternative-buffer attempts, however, the J_{sc} gain was accompanied by a V_{oc} loss, resulting in some degree of performance loss. In order to better understand the impact of RbF-PDT, we analyze a combination of experimental devices produced in the same in-line CIGS run with and without RbF-PDT in combination with chemical-bath-deposited CdS and Zn(O,S) buffers. Low-temperature current–voltage curves indicate a difference in Rb impact on the CIGS/CdS and CIGS/Zn(O,S) p-n junctions. For example, the diode-current barrier which creates a rollover often observed in RbF-treated CIGS/CdS current–voltage curves is significantly reduced for the CIGS/Zn(O,S) junction. Although the RbF-PDT had a positive impact on both junction partner combinations, the CIGS/Zn(O,S) devices' V_{oc} and fill factor (FF) benefited stronger from the RbF treatment. As a result, in our samples, the J_{sc} and FF gain balanced the V_{oc} loss, thus reducing the efficiency difference between cells with CdS and Zn(O,S) buffers.

Keywords: CIGS solar cells / RbF-PDT / Zn(O,S) / characterization

1 Introduction

Photovoltaic devices based on Cu(In,Ga)Se_2 (CIGS) absorbers have achieved higher conversion efficiencies than any other thin-film technology. All of the best performing devices in the last years used heavy alkali treatments, such as: Cs [1,2], Rb [3], or K [4,5].

While the advantage of the RbF treatment for CIGS performance is undeniable, multiple open questions concerning its impact on material and device properties still remain. Previous studies observed mainly an open-circuit voltage enhancement, which was sometimes accompanied by a FF loss [6–9]. The voltage increase could be attributed to an increased carrier density [6,7], a reduced defect density [6], grain boundary passivation [10–12], and/or due to $RbInSe_2$ formation at the interface [9,13,14].

Most of the previous work has concentrated on the impact of RbF treatment on a p-n junction formed by CIGS and CdS partners. When the buffer layer is exchanged, a different p-n junction is formed, which, in addition to a new interface with completely different properties, has also a different band alignment and band bending in the materials. One can expect a different impact of Rb on this junction. Therefore, in this work, we analyze how RbF impacts the CIGS/Zn(O,S) cell and compare it with a CIGS/CdS solar cell.

2 Sample description

The Cu(In,Ga)Se_2 absorber is deposited by co-evaporation of the elements in an inline system at ZSW, which closely resembles an industrial production process. Molybdenum-coated soda-lime glass substrates up to 30×30 cm^2 are transported on carriers, starting from an evacuated magazine. A continuous substrate flow is established and transports the carriers at a constant speed through a long vacuum chamber with up to five evaporation units. In these units, self-constructed evaporation sources deposit the elements in a line-shaped profile homogeneously from the top in a typical multi-stage process. In, Ga and Se are deposited in the first unit, followed in the second unit by Cu and Se to achieve a Cu-rich intermediate phase and then In, Ga and Se until the final Cu-poor composition is attained. The substrate heater temperatures are approximately 450 °C and 650 °C for units one and two, respectively. The 2–2.5-μm-thick CIGS layer grows in approximately 26 minutes. After cooling down in the next two units, the

* e-mail: ana.kanevce@zsw-bw.de

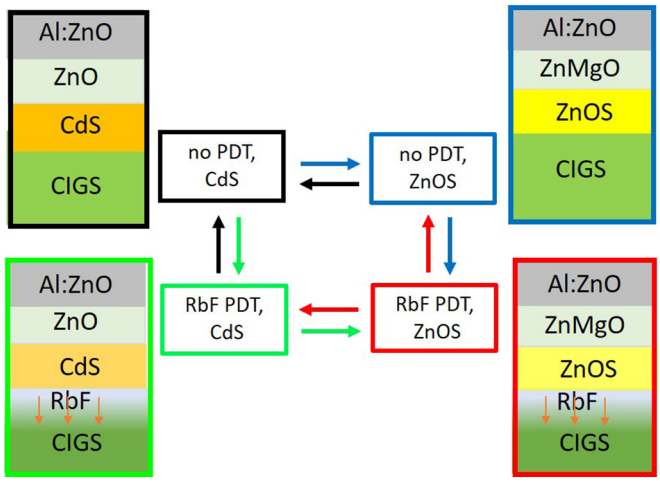

Fig. 1. The architectures and relationships between the four types of cells analyzed in this study.

substrates are transported through unit five, where RbF and Se can be evaporated as a PDT process. For the preparation of samples without and with PDT in the same deposition run, like in this study, the first carriers are coated with CIGS without PDT and only then the RbF source temperature is ramped up. The subsequent carriers are thus coated with nominally the same CIGS followed by an in-situ PDT process. Finally, the line of carriers is separated again and they are collected in a magazine in vacuum.

The analyzed cell architectures are shown in Figure 1. The first set has a 'standard' CIGS/CdS/i-ZnO/Al:ZnO architecture. On the top of the absorber layer, a 50-nm thick CdS buffer is deposited by chemical bath deposition (CBD) followed by an 80-nm thick undoped ZnO layer by RF sputtering, and a 400-nm thick Al-doped ZnO window layer by DC sputtering. Although further efficiency gains related to RbF-PDT are possible through a thinner CdS layer, here we kept the thickness at 50 nm for both PDT-treated and non-treated samples in order to maintain maximum comparability. In the second architecture, CIGS/Zn(O,S)/ZnMgO/Al:ZnO, the Zn(O,S) buffer is 25-nm thick and deposited by CBD as well, while the 80-nm thick $Zn_{0.75}Mg_{0.25}O$ and the 400-nm thick Al:ZnO window layers are RF and DC sputtered, respectively. The Zn(O,S) layer thickness was also kept constant for both CIGS with and without RbF-PDT in order to maintain maximum comparability. Both, the CdS and the Zn(O,S) layers, were deposited by a thiourea-based recipe [15].

The four different types of samples (Fig. 1) allow us to compare (vertically) the impact of RbF-PDT on the CIGS/CdS junction and CIGS/Zn(O,S) junction, or, comparing in a horizontal direction, the result of buffer change in samples with and without RbF-PDT, respectively. The color coding shown in Figure 1 will be carried throughout the paper.

3 Results

The solar-cell parameters of different types of cells are summarized in Figure 2. The substitution of CdS with Zn(O,S) results in a V_{oc} decrease, as commonly observed. The V_{oc} decrease, however, is lower for RbF-treated cells compared to the non-treated ones. The J_{sc} increase observed due to buffer substitution (Fig. 2b) appears equal in both cell types (independent of the RbF treatment) and is likely only due to the higher optical transparency of Zn(O,S). In this sample set we observe a decrease in J_{sc} for both buffers with PDT. However, this is not representative of the trend we normally see, which statistically shows no impact on J_{sc} due to RbF PDT.

As opposed to the non-PDT-treated cells, where the fill factor (FF) showed a slight decrease with the buffer change (black to blue in Fig. 2c), cells with the RbF treatment demonstrate a slightly improved FF for Zn(O,S) samples (green to red in Fig. 2c). And finally, due to the lower V_{oc} loss and FF increase, the efficiency of RbF-PDT-treated cells with Zn(O,S) buffer is not inferior to the ones with CdS. This suggests that RbF-PDT plays a significant and likely a more important role for the CIGS/Zn(O,S) junction in comparison to CIGS/CdS. In order to better understand this finding, we performed in-depth analyses with capacitance–voltage (CV) at room temperature and temperature-dependent current–density voltage (JV) on selected devices.

Figure 3a shows CV data for the different types of cells. The RbF-treated samples have an increased apparent carrier density, as expected. The apparent carrier density of the RbF-treated absorbers is comparable, regardless of the buffer type. However, the samples without PDT demonstrate a lower apparent carrier density for the Zn(O,S) buffer layer as compared to the CdS ones. Figure 3b shows the V_{oc} dependence on temperature for the different cell types. For three types of cells (no PDT/CdS, RbF/CdS and RbF/Zn(O,S)), V_{oc} extrapolation to 0 K yields the same value, indicating an equal activation energy. For the cell with Zn(O,S) buffer, which has not undergone the PDT treatment, the $V_{oc}(T)$ intercept is at a lower value. This result points towards a lower activation energy for recombination, which is typically attributed to a significant impact of interface recombination on device performance.

Next, we look at the evolution of the current–density voltage curves' shape with decreased temperature. The standard device, with a CdS buffer and without a PDT treatment, showed a well-behaved diode behavior throughout the temperature range (not shown). All of the other cells, however, showed signatures of secondary barriers as the temperature decreased. Light JV curves for different temperatures for RbF-PDT/CdS cells are shown in Figure 4a, while the light and dark JV curves at $T = 130$ K are shown in Figures 4b and 4c. As the temperature decreases, the JV curves for RbF-PDT/CdS samples show an impeded current collection in the forward direction, referred to as a rollover (also observed in Ref. [7]), which is more severe as the temperature drops. The source of rollover could be assigned to one (or both) of two locations, either to the back contact or to the p-n junction. A secondary barrier at the *p*-*n* junction can be formed: (i) at the CIGS/CdS interface, (ii) in the CdS, or (iii) at the CdS/ZnO interface.

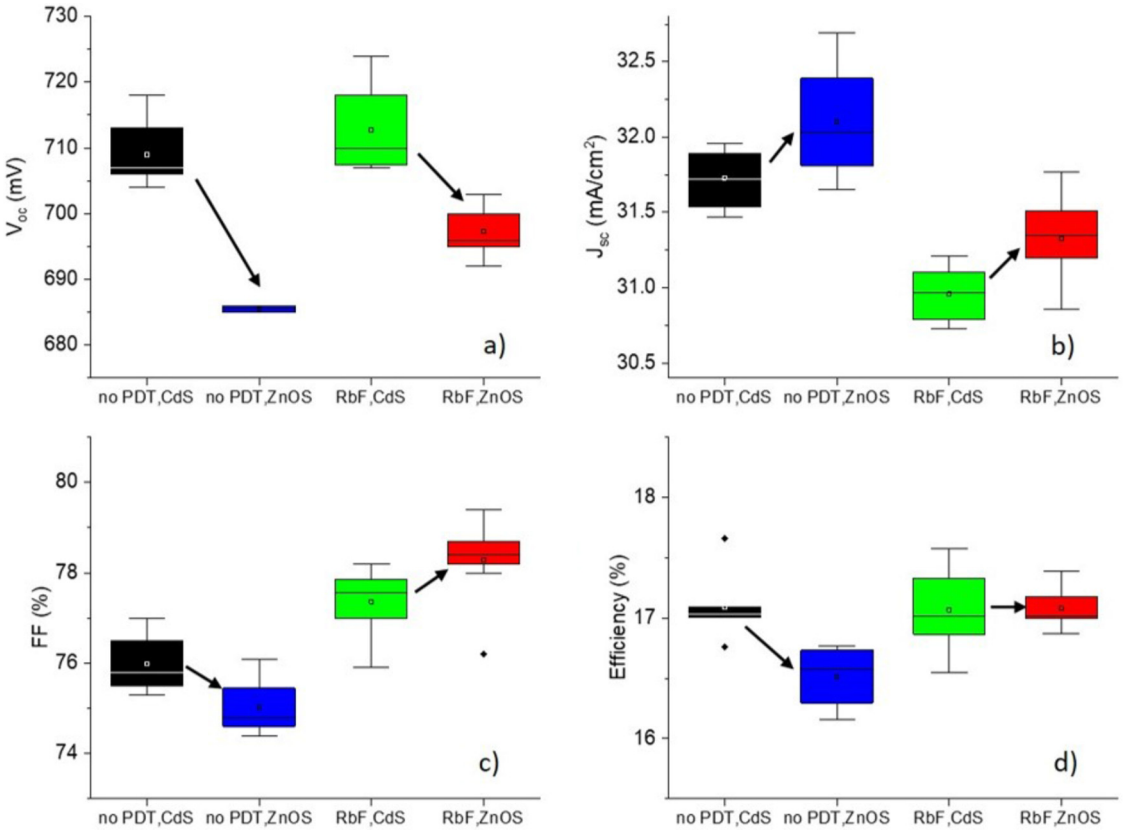

Fig. 2. V_{oc}, J_{sc}, FF and conversion efficiency for the four different types of cells. The box plots include 8–10 cells of each type.

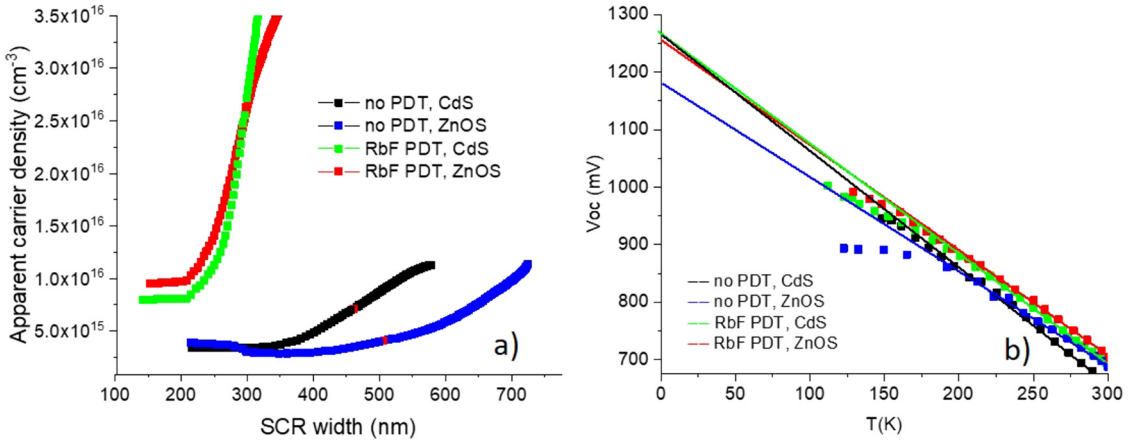

Fig. 3. (a) Apparent carrier density from the capacitance–voltage measurement. (b) V_{oc} as a function of temperature for different cell types.

Regardless of its exact cause, any type of a barrier at the CIGS/CdS interface, in addition to carrier impediment in forward direction, would also impede the photoelectron collection, and thus decrease the FF. However, by comparison of the black and the green curves in Figure 4b, one sees that the FF is similar despite the RbF treatment, which eliminates the hypotheses (i) and (ii). This leaves the CdS/ZnO interface and the back contact as possible sources for rollover. A CdS/ZnO barrier supports the observations by reference [7,11] as well. The JV curve of a RbF-treated cell with a Zn(O,S) buffer layer is shown in red in Figure 4b. By comparison of the green and red curves, one sees that the buffer substitution has changed the secondary barrier properties and the rollover is significantly reduced, while a small FF loss has appeared. This result supports the conclusion that the main reason for the rollover lies indeed in the CdS/i-ZnO interface, and not at the back contact.

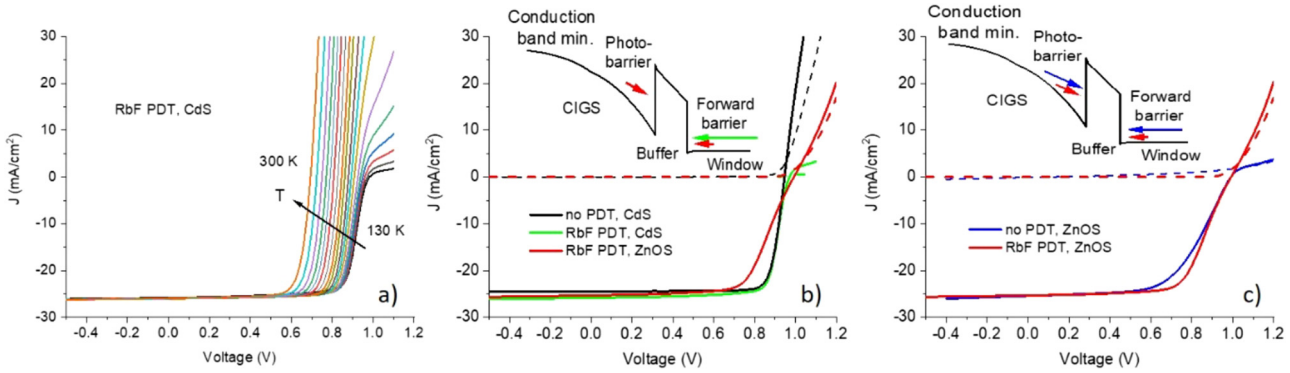

Fig. 4. (a) Light current–voltage curves for a RbF-PDT/CdS sample at different temperatures. (b) and (c) Light and dark current–voltage curves at $T = 130\,\mathrm{K}$ with descriptive band diagrams of the conduction band zoomed at the interface.

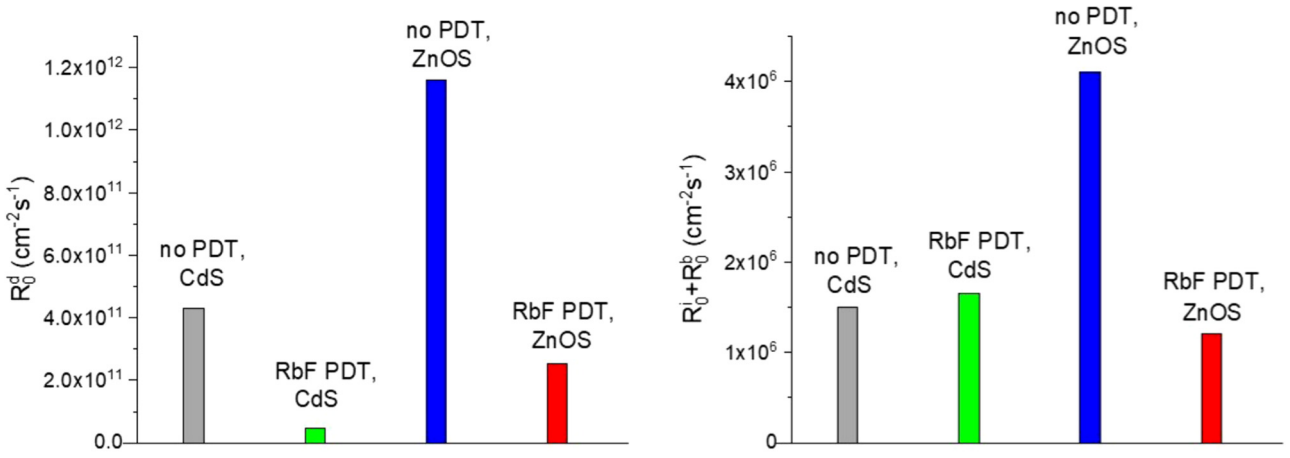

Fig. 5. Calculated recombination coefficients based on Grover-Li method for the four different types of cells.

JV curves at low temperatures for the RbF-treated and non-treated cells with Zn(O,S) buffer are shown in Figure 4c. The blue curve (non-PDT sample) shows a barrier in both directions which could indeed lie either in the buffer or at CIGS/Zn(O,S) interface. At this point we are not ready to speculate its origin. After the RbF-treatment (red curve), both of the barriers are improved. The barrier reduction might be an explanation for the FF improvement at room temperature due to RbF-treatment (Fig. 2).

To further analyze the impact of RbF-PDT on cells with different junction partners, JV curves at different illumination intensities (from 1 sun to 0.1 suns) were measured and recombination analysis as developed by Grover and Li [16,17] was performed. The recombination coefficients derived from these analyses are shown in Figure 5. The recombination coefficient in the space-charge region (SCR), $R_0{}^d$, is strongly decreased by the RbF-PDT, by a factor of 5 for the CIGS/CdS junction, and by almost a factor of 10 for the CIGS/Zn(O,S) junction. While the higher carrier density in the RbF-treated samples decreasing the SCR width by a factor of 2 (Fig. 3a) can explain the decrease of the $R_0{}^d$ by half, there is obviously an additional recombination passivation caused by RbF-PDT. In addition, the recombination in the depletion region is higher for the samples with Zn(O,S) buffers compared to the samples with CdS buffers.

$R_0{}^i + R_0{}^b$ increases only slightly due RbF-PDT in CdS cells, probably because of the SCR width decrease. In RbF-treated cells with Zn(O,S) buffers, however, the $R_0{}^i + R_0{}^b$ is decreased by a factor of 3 after the treatment. As the bulk properties in both samples are assumed to be equivalent, we believe that this is due to interface passivation. This interpretation is in agreement with the $V_{oc}(T)$ data shown in Figure 3b and with the previous research, where a downshifting of the bands due to the RbF-PDT was postulated [18,19]. This could decrease the hole supply at the CIGS/Zn(O,S) interface, and thereby reduce interface recombination.

4 Conclusions

We prepared CIGS solar cells with limited process variation to enable meaningful characterization and analysis of RbF-treated cells with CdS and Zn(O,S) buffer layers and compared with non-PDT-treated counterparts. Although the RbF-PDT had a positive impact on both junction partner combinations, the CIGS/Zn(O,S) devices' V_{oc} and FF benefited stronger from the RbF treatment. As

a result, in our samples, the J_{sc} and FF gain balanced the V_{oc} loss, thus reducing the efficiency advantage of CdS over the Zn(O,S) buffer. The low-temperature current–voltage curves showed a strong rollover for RbF-treated CIGS/CdS cells, which was significantly reduced by the buffer replacement, proving that the dominant barrier is in the junction, and not at the back contact. RbF treatment significantly decreases both the photoelectron and forward barriers for CIGS/Zn(O,S) cells. In addition, in cells with Zn(O,S) buffers, RbF-PDT decreases the recombination in the SCR as well as at the interface. RbF-PDT is more beneficial for the CIGS/Zn(O,S) junction, and its further optimization has a strong potential.

We thankfully acknowledge the funding by the German Federal Ministry of Economic Affairs and Energy (BMWi) under contract no. 0324179 (CISHiTec).

References

1. Solar Frontier, Solar Frontier Achieves World Record Thin-Film Solar Cell Efficiency of 23.35%, http://www.solar-frontier.com/eng/news/2019/0117_press.html
2. M. Nakamura et al., in *46th IEEE PVSC* (2019)
3. P. Jackson et al., Phys. Status Solidi RRL **10**, 583 (2016)
4. A. Chirila et al., Nat. Mater. **12**, 1107 (2013)
5. P. Jackson et al., Phys. Status Solidi RRL **8**, 219 (2014)
6. S. Karki et al., IEEE J. Photovolt. **9**, 1 (2019)
7. S. Kodalle et al., Sol. RRL **2**, 1800156 (2018)
8. T.P. Weiss et al., Adv. Mater. Interfaces **5**, 1701007 (2018)
9. S. Ishizuka et al., J. Phys. Chem. C **122**, 3809 (2018)
10. P. Schoeppe et al., Nano Energy **42**, 307 (2017)
11. S. Siebentritt et al., Adv. Energy Mater. **10**, 1903752 (2020)
12. A. Vilalta-Clemente et al., Appl. Phys. Lett. **112**, 103105 (2018)
13. N. Taguchi et al., Appl. Phys. Lett. **113**, 113903 (2018)
14. M. Malitckaya et al., J. Phys. Chem. C **121**, 15516 (2017)
15. D. Hariskos et al., IEEE J. Photovolt. **6**, 1321 (2016)
16. S. Grover et al., Appl. Phys. Lett. **103**, 093502 (2012)
17. J.V. Li et al., Sol. Energy Mater. Sol. Cells **124**, 143 (2014)
18. E. Handick et al., ACS Appl. Mater. Interfaces **7**, 27414 (2015)
19. D. Hauschild et al., ACS Energy Lett. **2**, 2383 (2017)

Cite this article as: Ana Kanevce, Stefan Paetel, Dimitrios Hariskos, Theresa Magorian Friedlmeier, Impact of RbF-PDT on Cu(In,Ga)Se_2 solar cells with CdS and Zn(O,S) buffer layers, EPJ Photovoltaics **11**, 8 (2020)